Tracking Tremor Frequency in Spike Trains Using the Extended Kalman Smoother

Sunghan Kim*, *Student Member, IEEE*, and James McNames, *Senior Member, IEEE*

***Abstract*—Tremor is one of the most disabling symptoms in patients with many movement disorders including Parkinson's disease (PD) and essential tremor (ET). Neural tremor manifests itself as a quasi-periodic fluctuation of the firing rate. We describe a frequency tracking method based on the extended Kalman smoother (EKS) to estimate the instantaneous tremor frequency (ITF) exhibited in binary spike trains detected from neural recordings. Simulation results demonstrate that the EKS frequency tracker can estimate the ITF accurately, even though the signal of interest is not sinusoidal and the noise is not Gaussian. The EKS frequency tracker can obtain a normalized mean squared error (NMSE) as low as 0.1 and performs much better than the conventional approach based on the Hilbert transform.**

***Index Terms*—Binary spike trains, essential tremor (ET), extended Kalman filter (EKF), Hilbert transform, instantaneous frequency, interspike interval, microelectrode recordings (MER), renewal process, spike detection, Parkinson's disease (PD).**

I. Introduction

TREMOR activity can be measured with many types of instrumentation and sensors including electroencephalograms (EEGs), magnetoencephalograms (MEGs), electromyograms (EMGs), accelerometers, and microelectrode recordings (MERs). Most tremor signals are quasi-periodic and nearly sinusoidal.

A number of recent studies have focused on characterizing the relationship of two or more tremor signals. In many cases, these signals are obtained from different types of instrumentation (e.g., MER and EMG). One of the surprising findings of these studies is that even when two signals contain significant tremor at the same frequency, these signals are not always coherent or phase coupled [1], [2]. This suggests that tremor either originates from multiple sources or that the tremor is modulated by uncoupled sources of unknown origin. A few studies have also found that the phase coupling between pairs of tremor signals varies over time [2]–[5].

One of the difficulties with studying phase coupling is that this signal behavior cannot be characterized with traditional signal processing and time series analysis techniques that assume that the signals are generated by a linear stochastic process. These methods are essentially blind to subtle nonlinear effects, such as intermittent phase coupling. This presents an opportunity for new signal processing methods that can estimate how the degree of phase coupling between pairs of tremor signals varies over time. Tracking the instantaneous tremor frequency (ITF) is a critical step in this type of analysis.

The objective of this work was to design a frequency tracker that estimates the ITF exhibited by neural recordings. These are widely modeled as point processes consisting of a series of action potentials, or spikes, that are treated as all-or-none events. Most researchers assume that all of the useful information is conveyed in the timing of these events. It is common practice to detect spikes during the early stages of analysis and focus all subsequent analysis on binary spike trains that consist of a 1 at the time of each spike occurrence and 0 elsewhere. Tremor is exhibited in this signal through pulse frequency modulation that causes fluctuations in the mean firing rate [6].

Hurtado *et al.* [2] conducted the most thorough study of intermittent coupling of tremor signals to date. They relied on the Hilbert transform (HT) to estimate Gabor's "analytic signal" and track the ITF. In practice, spike trains rarely meet the conditions necessary for this estimate to be accurate [7]. In particular, the representation of spikes as impulses results in a broad signal bandwidth that makes it difficult to track a single frequency.

Although the Kalman filter is not widely used for frequency tracking, it is a suitable approach for this problem because it is based on an explicit statistical model of the signal that permits the user to incorporate domain knowledge elegantly into the estimator. For example, in this application the observation noise in the binary spike trains, the amplitude and rate at which the tremor frequency fluctuates, and the typical range of tremor frequencies is either known or can be estimated. Since the ITF has a nonlinear relationship with the signal, we applied the extended Kalman smoother (EKS), which uses a first-order Taylor series approximation around estimates of the current state.

Several previous groups have applied the extended Kalman filter (EKF) to estimate the instantaneous frequency of sinusoidal or quasi-periodic signals in white Gaussian noise [8]–[10]. In this case, the EKF is closely related to the digital phase-locked loop [11]–[13]. In an earlier paper, we demonstrated the feasibility of tracking the ITF in binary spike trains with a traditional EKF [14]. We are not aware of any papers that describe how the EKF or EKS can be applied to nonsinusoidal signals or signals with non-Gaussian noise.

In this paper, we describe a new statistical signal model for use with the EKS that explicitly incorporates domain knowledge about tremor signals and that is more stable than the statistical model used in previous studies. We characterized its performance with synthetic binary spike trains in which the true ITF is known [6], [15]. We also demonstrate its performance on

Manuscript received July 21, 2005; revised February 5, 2006. *Asterisk indicates corresponding author.*

*S. Kim is with the Biomedical Signal Processing Laboratory, Department of Electrical & Computer Engineering, Portland State University, Portland, OR 97207 USA (e-mail: sunghan@pdx.edu).

J. McNames is with the Biomedical Signal Processing Laboratory, Department of Electrical & Computer Engineering, Portland State University, Portland, OR 97207 USA (e-mail: mcnames@pdx.edu).

Digital Object Identifier 10.1109/TBME.2006.877809

a real MER acquired from patients during stereotactic neurosurgery for Parkinson's disease and essential tremor.

II. Methodology

This section describes the design of the frequency tracker based on the EKS and the statistical model used to create synthetic binary spike trains with a known ITF.

A. Statistical Model

The Kalman filter recursively estimates the state of a linear stochastic process such that the mean squared error is minimized [16]. The Kalman smoother is a noncausal estimator that uses the entire record to estimate the state of a linear stochastic process. The extended versions of the Kalman filter and smoother are generalizations to the case of a nonlinear state space model that use a local linear approximation of the model. Since each updated estimate of the state is computed based on the previous state and the current values of the observed signal, the storage and computational requirements are manageable for most applications. The EKS is necessary for our application because the ITF has a nonlinear relationship with the binary spike train.

We use boldface notation to represent random processes, normal face for deterministic parameters, upper case letters for matrices, and lower case letters for vectors and scalars. The binary spike train is denoted as $\boldsymbol{b}(n)$ where $n = 0, \ldots, N$ is the independent variable representing discrete time. We define the centered binary spike train as our observed signal

$$\boldsymbol{y}(n) \triangleq \boldsymbol{b}(n) - \bar{b} \tag{1}$$

where $\bar{b}$ is the mean value of the $\boldsymbol{b}(n)$. Our statistical model for $\boldsymbol{y}(n)$ is

$$\boldsymbol{y}(n) = a\sin(2\pi T_{\mathrm{s}}\bar{f}n + \boldsymbol{\theta}(n)) + \boldsymbol{v}(n) \tag{2}$$

where $T_{\mathrm{s}} = 1/f_{\mathrm{s}}$ is the sampling interval, a is the amplitude of the sinusoidal component, $\bar{f}$ is the *a priori* estimate of the mean ITF provided by the user, and $\boldsymbol{v}(n)$ is a white noise process with zero-mean and variance r. The phase $\boldsymbol{\theta}(n)$ accounts for fluctuations in the ITF about the mean. If $\boldsymbol{\theta}(n) = 0$, then the ITF is constant. We model the instantaneous phase as a random walk driven by the fluctuations in the instantaneous frequency

$$\boldsymbol{\theta}(n+1) = \boldsymbol{\theta}(n) + 2\pi T_{\mathrm{s}} s\left[\frac{\boldsymbol{u}(n)}{2\pi}\right] \mod 2\pi. \tag{3}$$

The modulus operator has no affect on the model mathematically, but keeps $\boldsymbol{\theta}(n)$ bounded and reduces roundoff error. The instantaneous frequency of the process is defined as

$$\hat{\boldsymbol{f}}_{\mathrm{i}}(n) = \bar{f} + s\left[\frac{\hat{\boldsymbol{u}}(n)}{2\pi}\right] \tag{4}$$

where $s[\cdot]$ is a clipping function to prevent the ITF from exceeding user-specified limits, $f_{\min} \le \hat{f}_{\mathrm{i}} \le f_{\max}$

$$s[f] = \begin{cases} f_{\max} - \bar{f} & f_{\max} - \bar{f} \le f \\ f & f_{\min} - \bar{f} \le f < f_{\max} - \bar{f} \\ f_{\min} - \bar{f} & f < f_{\min} - \bar{f} \end{cases}. \tag{5}$$

This function also improves stability and robustness of the model because it limits the estimated ITF produced by the EKS to the range $f_{\min} \le \boldsymbol{f}_{\mathrm{i}}(n) \le f_{\max}$. When the EKS loses track of the ITF, this limits the range over which the estimate can diverge to and permits the EKS to regain track of the ITF more readily. If the actual range of the ITF is unknown, these limits can be effectively removed by selecting a very large range. The derivative of this function is given by

$$s'[f] \triangleq \frac{\mathrm{d}s[f]}{\mathrm{d}f} = \begin{cases} 1 & f_{\min} - \bar{f} \le f < f_{\max} - \bar{f} \\ 0 & \text{otherwise} \end{cases}. \tag{6}$$

We model $\boldsymbol{u}(n)$, which represents the fluctuations in ITF prior to clipping, as a first-order autoregressive (AR) process

$$\boldsymbol{u}(n+1) = \left(1 - \frac{2\pi f_u}{f_{\mathrm{s}}}\right)\boldsymbol{u}(n) + \boldsymbol{w}(n) \tag{7}$$

$$= \gamma\boldsymbol{u}(n) + \boldsymbol{w}(n) \tag{8}$$

where f_u is the cutoff frequency of the first-order AR process and $\boldsymbol{w}(n)$ is a white noise process with zero mean and variance $T_s q$. A value of $\gamma = 1$ results in a random walk model for the ITF and $\gamma = 0$ results in a white noise model of the ITF.

If we define the state vector $\boldsymbol{x}(n) \triangleq [\boldsymbol{\theta}(n)\ \ \boldsymbol{u}(n)]^{\mathrm{T}}$, then the state space model can be expressed as

$$\begin{aligned} \boldsymbol{x}(n+1) &= f(\boldsymbol{x}(n)) + G\boldsymbol{w}(n) \\ &= \begin{bmatrix} \boldsymbol{x}_1(n) + 2\pi T_{\mathrm{s}} s\left[\frac{1}{2\pi}\boldsymbol{x}_2(n)\right] & \mod 2\pi \\ \gamma\boldsymbol{x}_2(n) \end{bmatrix} \\ &\quad + \begin{bmatrix} 0 \\ 1 \end{bmatrix}\boldsymbol{w}(n) \\ \boldsymbol{y}(n) &= h_n(\boldsymbol{x}(n)) + \boldsymbol{v}(n) \\ &= a\sin(2\pi T_{\mathrm{s}}\bar{f}n + \boldsymbol{x}_1(n)) + \boldsymbol{v}(n). \end{aligned} \tag{9}$$

This state space model differs from prior work on the EKF for frequency tracking that used two state variables to represent the quadrature components [8]–[10], [14]. One problem with the quadrature model is that the measurement updates of the state estimates are not bounded. Since this knowledge is not included in the local linear approximations that the EKF state updates are based on, for some signal and parameter combinations, the EKF produces state estimates that diverge rapidly. The advantage of the model presented here and the estimate (4) is that they are always bounded. In this sense, these state update equations are more stable and robust to a wider range of user-specified parameters.

B. EKF

The EKF and EKS are based on local linear approximations of the state space model about an estimate of the state. Typically, the linearization is only performed during the filter portion of the algorithm. The output is linearized about the predicted estimate $\hat{\boldsymbol{x}}(n \mid n-1)$, a prediction of the state at time n given only the preceding observations $\{\boldsymbol{y}(n-1), \ldots, \boldsymbol{y}(0)\}$. The state prediction equation is linearized about the measurement update estimate $\hat{\boldsymbol{x}}(n \mid n)$, an estimate of the state given the current and preceding observations $\{\boldsymbol{y}(n), \ldots, \boldsymbol{y}(0)\}$. The EKS estimates are obtained from the EKF estimates. The EKF requires the user to provide an *a priori* estimate of the state and state error covariance matrix

$$\hat{\boldsymbol{x}}_{0 \mid -1} = 0 \quad P_{0 \mid -1} = \Pi_0. \tag{10}$$

The estimates of the ITF can then be computed with the EKF as follows:

$$\begin{aligned}
H_n &= [a\cos(\bar{\omega} n T_{\mathrm{s}} + \hat{\boldsymbol{x}}_1(n \mid n-1)) \quad 0] \\
r_{\mathrm{e},n} &= r + H_n P_{n \mid n-1} H_n^{\mathrm{T}} \\
K_{\mathrm{f},n} &= P_{n \mid n-1} H_n^{\mathrm{T}} r_{\mathrm{e},n}^{-1} \\
\hat{\boldsymbol{y}}(n \mid n-1) &= a\sin\left(\frac{2\pi \bar{f}}{f_{\mathrm{s}}} n + \hat{\boldsymbol{x}}_1(n \mid n-1)\right) \\
\boldsymbol{e}_n &= \boldsymbol{y}(n) - \hat{\boldsymbol{y}}(n \mid n-1) \\
\hat{\boldsymbol{x}}(n \mid n) &= \hat{\boldsymbol{x}}(n \mid n-1) + K_{\mathrm{f},n}(\boldsymbol{y}(n) - \hat{\boldsymbol{y}}(n \mid n-1)) \\
P_{n \mid n} &= P_{n \mid n-1} - K_{\mathrm{f},n} r_{\mathrm{e},n} K_{\mathrm{f},n}^{\mathrm{T}} \\
F_n &= \begin{bmatrix} 1 & 2\pi T_s s'[\hat{\boldsymbol{x}}_2(n \mid n)/(2\pi)] \\ 0 & \gamma \end{bmatrix} \\
P_{n+1 \mid n} &= F_n P_{n \mid n} F_n^{\mathrm{T}} + q T_{\mathrm{s}} \\
\hat{\boldsymbol{x}}(n+1 \mid n) &= \begin{bmatrix} \hat{\boldsymbol{x}}_1(n \mid n) + 2\pi T_{\mathrm{s}} s[\hat{\boldsymbol{x}}_2(n \mid n)/(2\pi)] \quad \mathrm{mod} 2\pi \\ \gamma \hat{\boldsymbol{x}}_2(n \mid n) \end{bmatrix} \\
\hat{\boldsymbol{f}}_{\mathrm{i}}(n \mid n) &= \bar{f} + s\left[\frac{\hat{\boldsymbol{x}}_2(n \mid n)}{2\pi}\right].
\end{aligned} \tag{11}$$

C. EKS

There are many mathematically equivalent expressions for the EKS. Here, we use a variant similar to that developed in [17] (see ([18], p. 374)). The EKS is initialized with

$$\boldsymbol{\psi}_{N+1 \mid N} = 0 \tag{12}$$

where $\boldsymbol{\psi}$ is called the adjoint variable.

The estimates of the ITF can then be computed with the EKS as follows:

$$\begin{aligned}
K_{\mathrm{p},n} &= \left(F_n P_{n \mid n-1} H_n^{\mathrm{T}}\right) r_{\mathrm{e},n}^{-1} \\
\boldsymbol{\psi}_{n \mid N} &= (F_n - K_{\mathrm{p},n} H_n)^{\mathrm{T}} \boldsymbol{\psi}_{n+1 \mid N} + H_n^{\mathrm{T}} r_{\mathrm{e},n}^{-1} \boldsymbol{e}_n \\
\hat{\boldsymbol{x}}_{n \mid N} &= \hat{\boldsymbol{x}}_{n \mid n-1} + P_{n \mid n-1} \boldsymbol{\psi}_{n \mid N} \\
\hat{\boldsymbol{f}}_{\mathrm{i}}(n \mid N) &= \bar{f} + s\left[\frac{\hat{\boldsymbol{x}}_2(n \mid N)}{2\pi}\right].
\end{aligned} \tag{13}$$

D. Parameter Selection

The statistical state space model in (9) has several parameters that must be specified or estimated before the EKF or EKS can be applied. The state space model was designed so that most of these parameters could be estimated based on domain knowledge. For example, the mean tremor frequency, $\bar{f}$, and range of possible frequencies, $f_{\min}$ and $f_{\max}$, are known from epidemiologic studies of tremor [19], [20].

The parameter γ controls the bandwidth of the AR process that models the ITF fluctuations. If $\gamma = 1$, $\boldsymbol{x}_3(n)$ becomes a random walk model. If $\gamma = 0$, $\boldsymbol{x}_3(n)$ is a white noise process. If $0 < \gamma < 1$, the modeled distribution of $\boldsymbol{x}_3(n)$ is centered at the mean tremor frequency $\bar{f}$. Smaller values of γ make it easier for the EKS to track frequencies that are close to $\bar{f}$, but make it more difficult to track frequencies that are far from $\bar{f}$. We used $\gamma = 0.9987$, which corresponds to a cutoff frequency of the AR process of $f_u = 0.2$ Hz.

The parameter a represents the amplitude of the ITF fundamental component in the centered binary spike train, $\boldsymbol{y}(n)$. Since $\boldsymbol{y}(n)$ is bounded, $-1 \leq \boldsymbol{y}(n) \leq 1$, the range of possible values of a is bounded as well. Empirically, the performance of the EKF/EKS frequency tracker is not sensitive to a, so a coarse estimate is usually sufficient. For the results in this paper we estimated a as

$$\hat{a} = \sqrt{2\hat{\sigma}_y^2 \frac{\int_{\omega_{\min}}^{\omega_{\max}} \hat{p}_y(\omega)\,\mathrm{d}\omega}{\int_0^{\pi} \hat{p}_y(\omega)\,\mathrm{d}\omega}} \tag{14}$$

where $\hat{\sigma}_y^2$ is the estimated variance of $\boldsymbol{y}(n)$ and $\hat{p}_y(\omega)$ is the estimated power spectral density of $\boldsymbol{y}(n)$. We used the Blackman-Tukey nonparametric estimator of the power spectral density with an autocorrelation window length of 5 s, a Blackman autocorrelation window [21], and a rectangular data window.

The EKS frequency tracker requires that the user provide an initial state vector, $\hat{\boldsymbol{x}}(0 \mid -1)$ and an initial estimate of the state covariance matrix, $P(0 \mid -1)$. The state vector can be initialized as $\hat{\boldsymbol{x}}(0 \mid -1) = [0\ 0]^{\mathrm{T}}$. In most applications, $P(0 \mid -1)$ is chosen as some scalar multiple of the identity matrix, $P(0 \mid -1) = \delta I$. Large and small values of δ indicate large and small degrees of uncertainty about the initial state, respectively. Practically, large values of δ may cause the EKS tracker to lock in more quickly, but may also cause the EKS tracker to be initially unstable and diverge rapidly from the initial state estimate. We used $\delta = 0.1$.

In a closely related state space model, [8] proved that the performance of the EKF frequency tracker depends primarily on the ratio $\lambda = r/q$. Empirically it appears that this applies to our state space model in (9) as well. This ratio determines how quickly the tracker adapts the state variables to changes in the observed signal. If λ is large, the tracker becomes sluggish, less sensitive to changes in $\boldsymbol{b}(n)$, and it is unable to track rapid changes in the ITF. If λ is small, the tracker becomes more sensitive to changes of the ITF, the estimated ITF is more variable, and it is more sensitive to artifact and noise, which may cause it to lose track of the ITF more often. Thus, λ is the primary parameter that controls the tradeoff between the bias and variance of the ITF estimate.

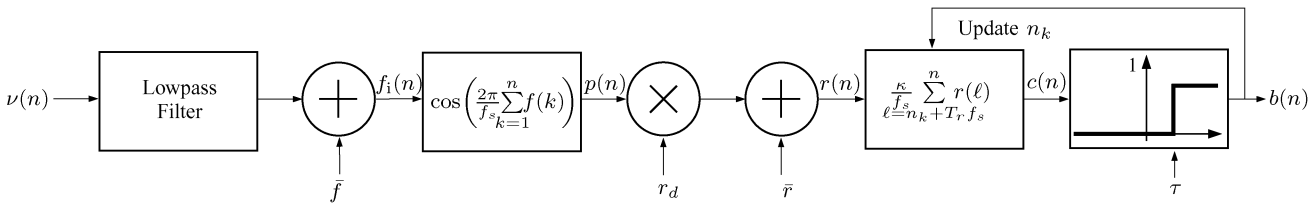

Fig. 1. Block diagram of the statistical model used to create synthetic binary spike trains with an ITF $\boldsymbol{f}_{\mathrm{i}}(n)$. The unscaled quasi-periodic component of the firing rate is represented as $\boldsymbol{p}(n)$, r_d determines how much this affects the instantaneous firing rate $\boldsymbol{r}(n)$, and $\bar{r}$ is the mean firing rate for the process. The summing block represents an integrate-and-fire model of neural activity with random thresholds τ selected from a gamma distribution. Further details of this model can be found in [6].

TABLE I
SUMMARY OF USER-SPECIFIED DESIGN PARAMETERS FOR THE EKS FREQUENCY TRACKER

Name	Symbol	Value
AR Cutoff Frequency	f_u	0.2 Hz
Measurement/process noise ratio	$\lambda = r/q$	100
Minimum possible frequency	$f_{\min}$	4 Hz
Maximum possible frequency	$f_{\max}$	12 Hz
Mean tremor frequency	$\bar{f}$	6 Hz
Initial covariance matrix	$P(0\|-1)$	$0.1I$

where I is the identity matrix.

Table I lists the design parameters we used for the results and examples in this paper. These values were selected to match what is known about the physiology of tremor in patients with essential tremor and based on empirical results obtained during the development of the tracker.

E. Synthetic Binary Spike Train With Tremor

With real binary spike trains there is no gold standard that can be used to assess the accuracy of the estimated ITF, so we used synthetic binary spike trains in which the true ITF is known. Fig. 1 shows a block diagram of the statistical model for binary spike train synthesis. The first two steps generate a known (or true) ITF, $\boldsymbol{f}_{\mathrm{i}}(n)$. This is used to create a quasi-periodic signal, $\boldsymbol{p}(n)$, which is scaled and added to a mean firing rate to create the instantaneous firing rate (IFR), $\boldsymbol{r}(n)$. The last two steps create a binary spike train based on an integrate-and-fire model of a renewal process [15]. The regularity of the firing rate is determined by the distribution of the random thresholds, τ [6].

1) Instantaneous Firing Rate Generation: We lowpass filtered white Gaussian noise $\boldsymbol{\nu}(n)$ with a low cutoff frequency, f_c, to create a stochastic ITF $\boldsymbol{f}_{\mathrm{i}}(n)$. The cutoff frequency should be small ($\leq$1 Hz) because the ITF of real tremor signals varies slowly over time. The variance of $\boldsymbol{\nu}(n)$, σ_ν^2, determines the variance of $\boldsymbol{f}_{\mathrm{i}}(n)$. We are not aware of any papers that characterize the bandwidth (f_c) and amplitude (σ_ν^2) of different types of ITFs so there is little domain knowledge, at present, to guide the selection of these parameter values. We chose $f_c = 0.5$ Hz and $\sigma_\nu^2 = 100$ Hz^2 based on a visual inspection of a time-frequency analysis of real ITFs.

The instantaneous phase is defined as the integral of the instantaneous frequency [7]. We estimate this integral with a Riemann sum

$$\boldsymbol{\phi}(n) = \frac{2\pi}{f_s}\sum_{k=1}^{n}\boldsymbol{f}(k) = \boldsymbol{\phi}(n-1) + \frac{2\pi}{f_s}\boldsymbol{f}_{\mathrm{i}}(n). \tag{15}$$

This is an accurate estimate because the sample rate (say $f_s = 1000$ Hz) is much larger than the bandwidth of the ITF (say $f_c = 0.5$ Hz). The instantaneous firing rate $\boldsymbol{r}(n)$, sometimes called the process intensity, is given by

$$\boldsymbol{r}(n) = \bar{r} + r_d\cos[\boldsymbol{\phi}(n)] \tag{16}$$

where $\bar{r}$ is the mean firing rate ($<$200 Hz) and r_d is the maximum deviation of the firing rate from $\bar{r}$. The modulation index is then defined as

$$m \triangleq \frac{r_d}{\bar{r}}. \tag{17}$$

One limitation of this model is that it assumes a constant amplitude of the fluctuations in $\boldsymbol{r}(n)$ due to tremor, which is controlled by r_d. We are not aware of any prior work that has investigated how r_d varies with time or the state of the patient. A constant amplitude model is a reasonable and sufficient approximation for this study.

2) Binary Spike Train Generation: The binary spike train $\boldsymbol{b}(n)$ was generated using an integrate-and-fire model of neural activity. The first step of this process integrates the instantaneous firing rate, $\boldsymbol{r}(n)$, until it reaches a random threshold, τ. When $\boldsymbol{r}(n) \geq \tau$, the statistical model creates an event (i.e., a spike) and resets the integral to zero. This is a type of renewal process because the time of the next event depends only on the time of the preceding event. Therefore, interspike intervals are statistically independent random variables, given that $\boldsymbol{r}(n)$ is known [15].

Similar to (15), we estimated the integral of the firing rate with a Riemann sum

$$\boldsymbol{c}(n) = \frac{\kappa}{f_s}\sum_{\ell=n_k+T_r f_s}^{n}\boldsymbol{r}(\ell) \tag{18}$$

TABLE II
SUMMARY OF USER-SPECIFIED DESIGN PARAMETERS FOR BINARY SPIKE TRAIN SYNTHESIS

Name	Symbol	Value
Variance of white Gaussian noise	σ_ν^2	100 Hz^2
Sample Rate	f_s	1000 Hz
Cutoff Frequency	f_c	0.5 Hz
Mean Tremor Frequency	$\bar{f}$	6 Hz
Signal Duration	T	30 s
Refractory Time	T_r	1 ms
Mean Firing Rate	$\bar{r}$	100 Hz
Modulation Index	$m = r_d/\bar{r}$	0.8
Threshold shape parameter	α	1

where $\boldsymbol{c}(n)$ is the integrated firing rate and n_k is the time of the preceding event. Real neurons have a brief refractory period after each spike. During this period neurons cannot produce another spike. We modeled this by excluding a period of T_r seconds from the cumulative sum in (18). The cumulative sum is scaled by κ so that the average intensity of the final recording, which includes these refractory periods with zero intensity, will be the same as the average of $\boldsymbol{r}(n)$ [15]

$$\kappa = \frac{1}{1 - T_r\bar{r}}. \tag{19}$$

The threshold τ is a continuous random variable drawn from a gamma distribution

$$f(\tau;\alpha,\beta) = \frac{x^{\alpha-1}\exp -\frac{x}{\beta}}{\beta^\alpha \Gamma(\alpha)} \quad x \in [0,\infty) \tag{20}$$

where α is the shape parameter, β is the scale parameter, and $\Gamma(\,\cdot\,)$ is the gamma function. We set β to α^{-1} so that the mean of τ is 1. When $\alpha = 1$, τ has an exponential distribution and the statistical model generates a Poisson process. As $\alpha > 1$, the distribution is more localized around its mean and the binary spike train becomes more regular and more dependent on $\boldsymbol{f}_{\mathrm{i}}(n)$. For large values $(\alpha \gg 1)$, the distribution of τ is approximately Gaussian with a variance $\sigma_\tau^2 = \alpha^{-1}$. When $\alpha < 1$, the binary spike train is less regular with many short intervals and few long ones and is less dependent on $\boldsymbol{f}_{\mathrm{i}}(n)$ [6], [15]. This resembles neuronal activity that contains bursts of spikes. We set $\alpha = 1$ (a Poisson process), which is the most common model of neural firing patterns.

Table II lists the parameter values that we used for our simulation results. These values were carefully chosen so that synthetic binary spike trains resemble real binary spike trains recorded from patients with essential tremor as closely as possible.

III. PERFORMANCE ASSESSMENT

The following sections show that the EKS frequency tracker can track the true ITF given only the binary spike train as the observed signal. We estimate the sensitivity of the tracker to some of the user-specified parameters and properties of the binary spike train with synthetic signals, and we demonstrate the EKS tracker's performance on real binary spike trains.

A. Comparator Tracking Algorithms

In all cases, we compare the performance of our frequency tracker to the HT frequency tracker and a simple peak picking algorithm applied to a spectrogram. For the HT frequency tracker we followed the methodology described in [2], [5] as closely as possible. Prior to the transform we filtered the signal with an FIR bandpass filter with a passband of 4–12 Hz and stopbands of 0–3 Hz and >13 Hz. The filter was specified to have >60 dB of attenuation in the lower stopband and >80 dB of attenuation in the upper stopband.

The third frequency tracker was based on the nonparametric spectrogram (NS). The distribution of the signal power in the time-frequency plane was estimated by using the modified periodogram to estimate the power spectral density of overlapping windowed segments of the observed signal. Edge conditions were handled by repeating the first and last values of the observed signal. To reduce high-frequency noise and decrease computation, the signal was decimated to a bandwidth of 0–25 Hz prior to estimation. Zero padding was used to increase the frequency resolution to $25/512 \approx 0.05$ Hz. Each windowed segment was 1.25 s in duration. We multiplied each segment by a Blackman window. We located the largest peak in the frequency range 4–12 Hz. The peaks were located in 400 overlapping segments uniformly distributed over the time span of the signal. We used a cubic smoothing spline with a smoothing parameter of 0.99 to interpolate the ITF to the signal sample rate ($f_{\mathrm{s}} = 1000$ Hz).

B. Performance Metric

We used normalized mean-square-error (NMSE) as our performance metric

$$\mathrm{NMSE} = \frac{\sum_{n=1}^{Tf_s}(\boldsymbol{f}_{\mathrm{i}}(n) - \hat{\boldsymbol{f}}_{\mathrm{i}}(n))^2}{\sum_{n=1}^{Tf_s}(\boldsymbol{f}_{\mathrm{i}}(n) - \bar{f})^2} \tag{21}$$

where $\boldsymbol{f}_{\mathrm{i}}(n)$ is the true ITF, $\hat{\boldsymbol{f}}_{\mathrm{i}}(n)$ is the estimated ITF, and $\bar{f}$ is the mean ITF. This is convenient metric because it has a natural scale. A value $\mathrm{NMSE} = 1$ means that the average accuracy of the estimated ITF is no better than simply using the mean ITF as an estimate. Values of $\mathrm{NMSE} > 1$ indicate poor frequency tracking and those of NMSE indicate accurate frequency tracking.

C. Synthetic Spike Train Examples

We generated synthetic binary spike trains with piecewise constant ITFs and with a stochastic ITF that changed slowly ($f_c = 0.5$ Hz). Figs. 2 and 3 show how well the EKS tracked these two types of ITFs.

In most previous work, the EKF has only been used to track the instantaneous frequency of sinusoidal signals contaminated with white Gaussian noise. The examples shown in Figs. 2 and 3 demonstrate that the EKS can track the ITF of binary spike trains even though the signal is not sinusoidal and the noise is not Gaussian. In both cases, $\mathrm{NMSE} < 0.12$ for the EKS tracker. The NS tracker had similar performance, but the HT tracker performed substantially worse.

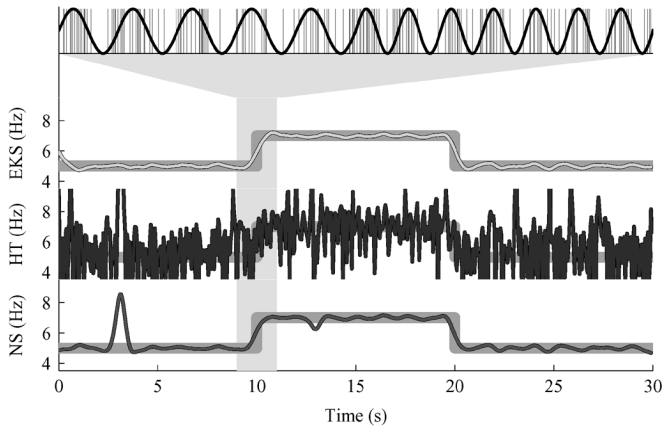

Fig. 2. Example of a synthetic spike train (top plot, vertical thin lines), the true process intensity $\boldsymbol{r}(n)$ (top plot, scaled sinusoid), the true and estimated ITFs by the EKS (upper, $\mathrm{NMSE} = 0.032$), HT (middle, $\mathrm{NMSE} = 13.7$), and NS (bottom, $\mathrm{NMSE} = 0.219$) frequency trackers. The ITF was piecewise constant with shifts from 5 to 7 Hz. The gray region shows the time span of the spike train.

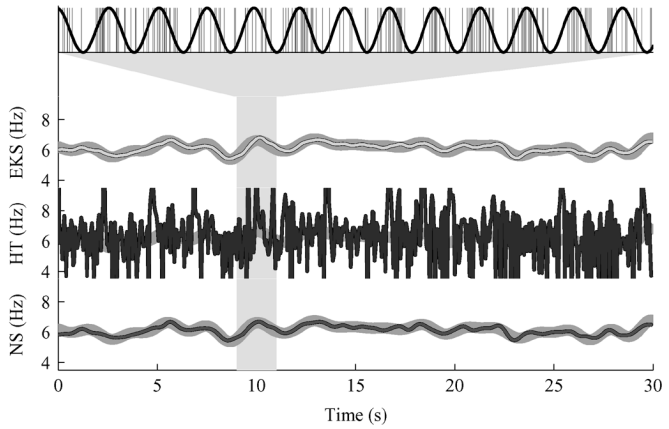

Fig. 3. Example of a synthetic spike train (top plot, vertical thin lines), the true process intensity $\boldsymbol{r}(n)$ (top plot, scaled sinusoid), the true and estimated ITFs by the EKS (upper, $\mathrm{NMSE} = 0.105$), HT (middle, $\mathrm{NMSE} = 175$), and NS (bottom, $\mathrm{NMSE} = 0.114$) frequency trackers. The ITF was a filtered white noise process with a cutoff frequency of $f_c = 0.5$ Hz. The gray region shows the time span of the spike train.

D. Performance Sensitivity to λ

The performance of the EKS tracker is sensitive to the parameter λ, and there is no domain knowledge that can be used to guide the selection of this parameter value. To determine the sensitivity of the EKS tracker to this parameter, we measured how the NMSE varied with λ.

Fig. 4(a) shows the sensitivity of the EKS tracker's performance to λ. The mean NMSE value over $n_s = 250$ simulations for each value of λ was less than 1 over a range of $-3 < \log_{10}\lambda < 1$ with a minimum of $\mathrm{NMSE} = 0.101 \pm 0.078$ (average $\pm$ standard deviation). The HT frequency tracker achieved $\mathrm{NMSE} = 129 \pm 54.6$ and the spectrogram achieved $\mathrm{NMSE} = 0.523 \pm 0.769$. Fig. 4(b)–(d) shows examples of how accurately the EKS tracks the ITF for a wide range of values of λ. These examples show that if λ is too large [Fig. 4(b)], the estimate has excessive bias that causes the estimate to be nearly constant and not track the ITF; if λ is too small [Fig. 4(d)], the estimate has excessive variance that causes it to frequently lose track; and if λ is appropriate [Fig. 4(c)], the estimate tracks the ITF accurately.

Fig. 4(d) shows the advantage of constraining the range of possible frequencies by (5). In this case, λ is too small and the tracker is too sensitive to random fluctuations in $\boldsymbol{y}(n)$. This causes the tracker to frequently lose track. However, the constrained frequency range enables the tracker to regain track more easily than is possible without clipping.

E. Performance Versus Strength of Tremor (Modulation Index m)

In order to investigate the relationship between the performance of a tremor tracking algorithm and the strength of the tremor signal, we measured the performance of the EKS tracker versus the modulation index m of the instantaneous firing rate $\boldsymbol{r}(n)$. The ITF can be more easily estimated when the tremor component of $\boldsymbol{r}(n)$ is larger (i.e., the modulation index m is close to 1).

Fig. 5 shows the NMSE of the EKS and NS trackers over a range of values of m. The performance of the HT frequency tracker is not shown here because the NMSE exceeded the range of the vertical scale ($\mathrm{NMSE} > 1.25$) for the entire range of m. The average performance at $m = 0.8$ was $\mathrm{NMSE} = 0.101 \pm 0.084$ (average $\pm$ standard deviation) for the EKS tracker, $\mathrm{NMSE} = 136 \pm 64.5$ for the HT tracker, and $\mathrm{NMSE} = 0.591 \pm 0.857$ for the NS tracker. Real binary spike trains with tremor have a large amplitude modulation index of nearly 1, so the region of good performance, $\mathrm{NMSE} < 0.2$ for $m > 0.7$, is well within the range of binary spike trains obtained from real neural recordings.

F. Real Tremor Example

Figs. 6 and 7 show examples of the EKS frequency tracker applied to binary spike trains recorded during stereotactic neurosurgery for patients with Parkinson's disease and essential tremor, respectively. We detected the spikes using an automatic spike detection algorithm similar to that in [22]. In both cases, the EKS tracker is able to track the ITF closely despite disturbances and time-varying amplitude. The spectrograms of the residuals show that the EKS tracker has effectively accounted for the tremor variation, though the fundamental is faintly visible in some regions due to the time-varying amplitude. In Fig. 7, the residuals are significant at the left edge during the period in which the tracker transitions from the *a priori* estimate of the ITF (6 Hz) to the actual ITF of this signal. Overall, the EKS tracker performed very well in these examples.

IV. Summary and Conclusion

We developed an EKS frequency tracking algorithm to estimate the ITF contained in binary spike trains. The simulation results demonstrate that the EKS frequency tracker can estimate the ITF accurately, even though the signal of interest is not sinusoidal and the noise is not Gaussian. We also demonstrated the accuracy of the EKS frequency tracker on a binary spike train detected from real MERs obtained from patients with Parkinson's disease and essential tremor.

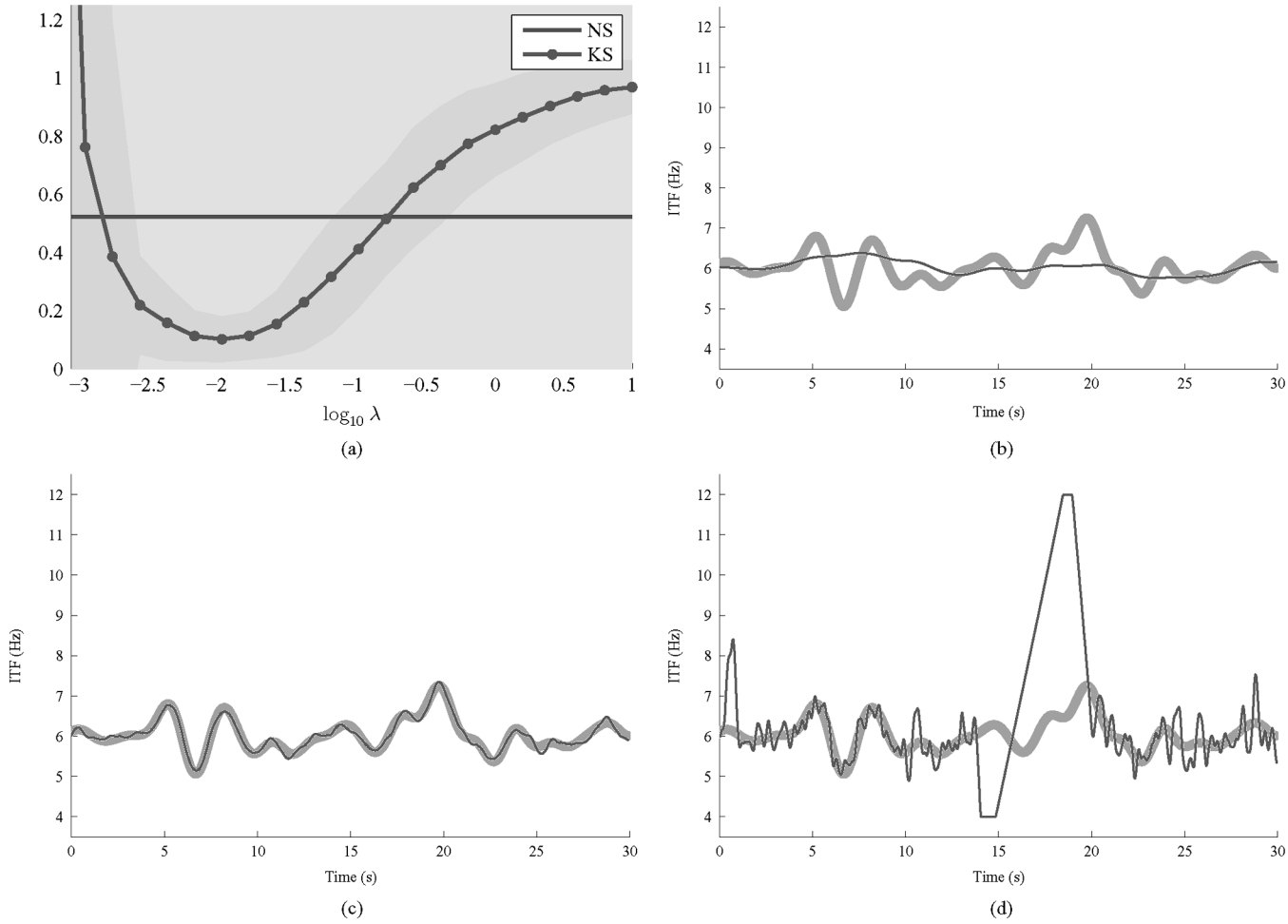

Fig. 4. (a) Performance of the EKS and NS trackers versus the variance ratio λ. The dark line is the average NMSE calculated from 250 simulations at each value of λ. The shaded regions represent one standard deviation above and below the mean. (b)–(d) True tremor frequency (thick, gray line) and the estimated ITF (thin, green line) for three different values of λ. (a) NMSE versus λ, (b) $\log_{10}\lambda = -1$, (c) $\log_{10}\lambda = -2$, and (d) $\log_{10}\lambda = -3.5$.

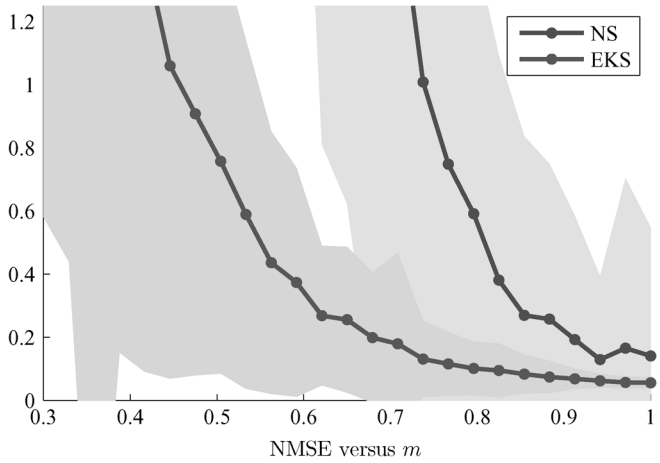

Fig. 5. NMSE of the EKS and NS frequency trackers over a range of values of m. The dark lines show the mean NMSE and the shaded regions show the corresponding standard deviations. The means and standard deviations were estimated from 250 simulations for each value of m.

In all of our results, the EKS frequency tracker performed substantially better than the HT frequency tracker. The HT tracker performed poorly in large part because the signal power is not sufficiently concentrated in the time-frequency plane [7]. Rather, the binary spike train representation of a signal spreads the signal power over a broad range of frequencies. This could be partly remedied by using bandpass filter with a smaller passband, as done in [2] and [5] (2–6 Hz instead of 4–12 Hz). The synthetic examples with known ITF also suggest that the HT frequency tracker can generate gross errors that may be misidentified as phase slips in real signals.

The EKS frequency tracker performs well because of many of the features that we incorporated into the design. Many of the model parameters can be chosen based on domain knowledge. The state space model uses a more stable representation of a quasi-periodic sinusoid than previous state space models with a quadrature representation. Our model ensures that the state estimate for the phase and our estimate of the ITF are bounded. The instantaneous frequency uses an AR model, rather than a random walk model, to encourage the estimates to be near the mean tremor frequency, which is usually known from domain knowledge. Clipping is used for similar reasons and also helps the EKS tracker regain frequency lock more easily. Collectively these features result in an accurate frequency tracker that can be used in subsequent studies to better understand the pathophysiology of tremor.

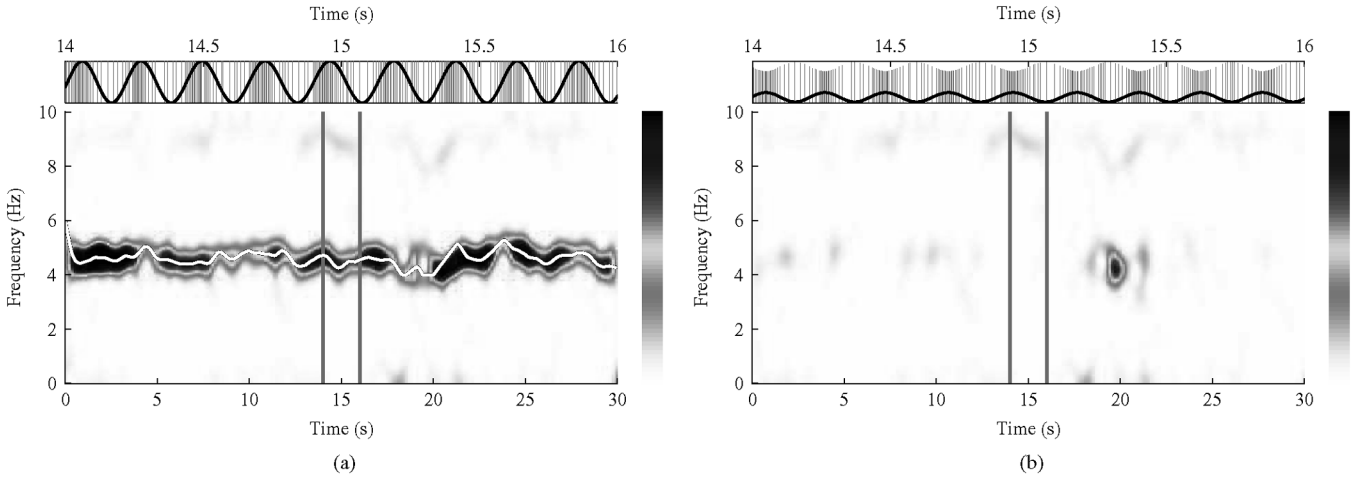

Fig. 6. (a) Spectrogram of spike trains obtained from MERs recorded during stereotactic neurosurgery for Parkinson's disease. The tremor is shown by the dark horizontal band. The ITF estimated by the EKS frequency tracker is shown by the white trace overlayed on the spectrogram. A 2-s segment of the spike train is shown in the top figure along with the quasi-periodic sinusoid (scaled) estimated by the EKS frequency tracker. The time span of the spike train segment is shown by the vertical gray lines on the spectrogram. (b) Spectrogram of the residuals after removing the smoothed estimates of the tremor fundamental component of the spike trains. The top plot shows the spike train with the estimated component removed and the estimated tremor fundamental component. (a)Parkinson's disease estimate, (b) Parkinson's disease residuals.

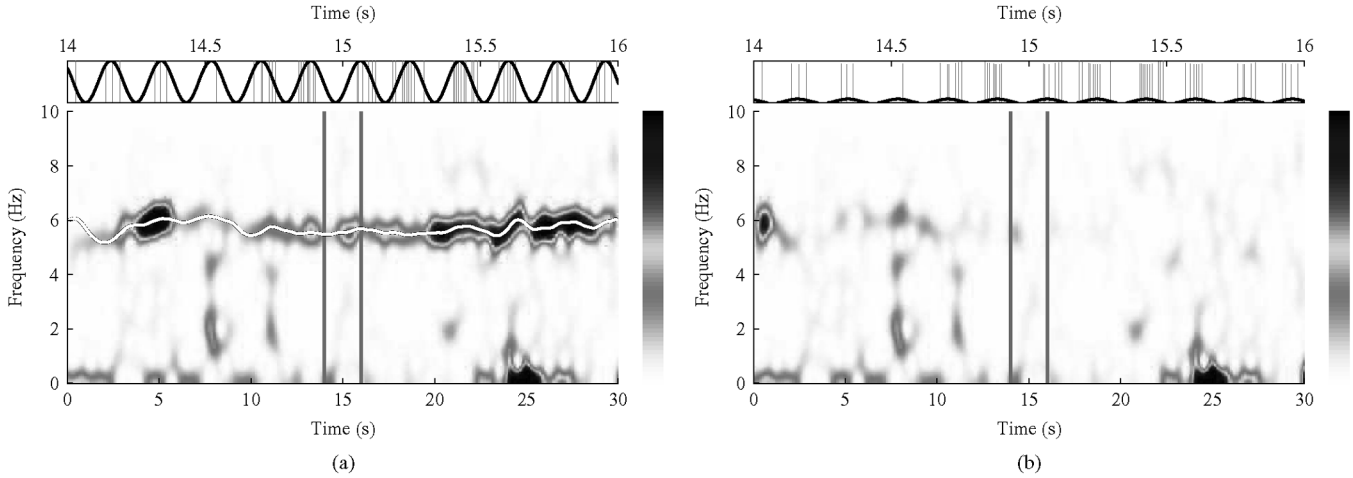

Fig. 7. (a) Spectrogram of spike trains obtained from MERs recorded during stereotactic neurosurgery for essential tremor. The tremor is shown by the dark horizontal band. The ITF estimated by the EKS frequency tracker is shown by the white trace overlayed on the spectrogram. A 2-s segment of the spike train is shown in the top figure along with the quasi-periodic sinusoid (scaled) estimated by the EKS frequency tracker. The time span of the spike train segment is shown by the vertical gray lines on the spectrogram. (b) Spectrogram of the residuals after removing the smoothed estimates of the tremor fundamental component of the spike trains. The top plot shows the spike train with the estimated component removed and the estimated tremor fundamental component. (a) Essential tremor estimate, (b) Essential tremor residuals.

REFERENCES

[1] J. M. Hurtado, J.-P. Lachaux, D. J. Beckley, C. M. Gray, and K. A. Sigvardt, "Inter- and intralimb oscillator coupling in Parkinsonian tremor," *Movement Disorders*, vol. 15, no. 4, pp. 683–691, 2000.

[2] J. M. Hurtado, L. L. Rubchinsky, K. A. Sigvardt, V. L. Wheelock, and C. T. Pappas, "Temporal evolution of oscillations and synchrony in gpi/muslce pairs in Parkinson's disease," *J. Neurophysiol.*, vol. 93, no. 3, pp. 1569–1584, Mar. 2005.

[3] J. M. Hurtado, C. M. Gray, L. B. Tamas, and K. A. Sigvardt, "Dynamics of tremor-related oscillations in the human globus pallidus: A single case study," *Proc. Nat. Acad. Sci. USA*, vol. 96, no. 4, pp. 1674–1679, Feb. 1999.

[4] B. Hellwig, B. Schelter, B. Guschlbauer, J. Timmer, and C. H. Lücking, "Dynamic synchronization of central oscillators in essential tremor," *Clin. Neurophysiol.*, vol. 114, pp. 1462–1467, 2003.

[5] J. M. Hurtado, L. L. Rubchinsky, and K. A. Sigvardt, "Statistical method for detection of phase-locking episodes in neural oscillations," *J. Neurophysiol.*, vol. 91, no. 4, pp. 1883–1898, Apr. 2004.

[6] J. McNames, "Pulse frequency demodulation without spike detection," in *Proc. 2nd Int. IEEE EMBS Conf. Neural Engineering*, Mar. 2005, pp. 229–232.

[7] B. Boashash, "Estimating and interpreting the instantaneous frequency of a signal—Part 1: Fundamentals," *Proc. IEEE*, vol. 80, no. 4, pp. 520–538, Apr. 1992.

[8] S. Bittanti and S. M. Savaresi, "On the parameterization and design of an extended Kalman filter frequency tracker," *IEEE Trans. Autom. Control*, vol. 45, no. 9, pp. 1718–1724, Sep. 2000.

[9] B. F. La Scala, R. R. Bitmead, and B. G. Quinn, "An exteded Kalman filter frequency tracker for high-noise environments," *IEEE Trans. Signal Process.*, vol. 44, no. 2, pp. 431–434, Feb. 1996.

[10] P. J. Parker and B. D. Anderson, "Frequency tracking of nonsinusoidal periodic signals in noise," *Signal Process.*, vol. 20, no. 2, pp. 127–152, Jun. 1990.

[11] C. N. Kelly and S. C. Gupta, "The digital phase-locked loop as a near-optimum FM demodulator," *IEEE Trans. Commun.*, vol. COM-20, no. 3, pp. 406–411, Jun. 1972.

[12] D. R. Polk and S. C. Gupta, "Quasi-optimum digital phase-locked loops," *IEEE Trans. Commun.*, vol. COM-21, no. 1, pp. 75–82, Jan. 1973.

[13] ——, "An approach to the analysis of performance of quasi-optimum digital phase-locked loops," *IEEE Trans. Commun.*, vol. COM-21, no. 6, pp. 733–738, Jun. 1973.

[14] S. Kim and J. McNames, "Tracking tremor frequency in spike trains using the extended Kalman filter," presented at the 27th Annu. Int. Conf. Engineering in Medicine and Biology Soc., Shanghai, China, Sep. 2005.
[15] D. H. Johnson, "Point process models of single-neuron discharges," *J. Computational Neurosci.*, vol. 3, no. 4, pp. 275–299, Dec. 1996.
[16] R. Kalman, "A new approach to linear filtering and prediction problems," *Tran. ASME—J. Basic Eng.*, ser. D, vol. 82, pp. 35–45, 1960.
[17] A. E. Bryson and M. Frazier, Smoothing for Linear and Nonlinear Dynamic Systems Ohio, 1963, Tech. Rep. TDR 63-119, Aero. Syst. Div. Wright-Patterson Air Force Base.
[18] T. Kailath, A. H. Sayed, and B. Hassibi, *Linear Estimation*. Upper Saddle River, NJ: Prentice-Hall, 2000.
[19] L. J. Findley, "Epidemiology and genetics of essential tremor," *Neurology*, vol. 54, no. 11, pp. S8–S13, Jun. 2000, Suppl. 4.
[20] G. Dëuschl and R. J. Elble, "The pathophysiology of essential tremor," *Neurology*, vol. 54, no. 11, pp. S14–S20, Jun. 2000, Suppl. 4.
[21] A. V. Oppenheim and R. W. Schafer, *Discrete-Time Signal Processing*, 2nd ed. Upper Saddle River, NJ: Prentice-Hall, 1999.
[22] S. Kim, J. McNames, and K. Burchiel, "Detecting tremors in microelectrode recordings without using a spike detector," in *Proc 26th Annu. Int. Conf. Engineering in Medicine and Biology Soc.*, 2004, vol. 1, pp. 357–360.

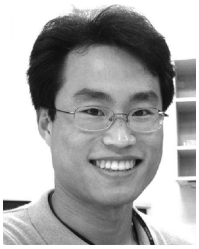

Sunghan Kim (SM'03) received the B.S. and M.S. degrees in electrical engineering from Portland State University, Portland, OR, in 2003 and 2005, respectively. He is currently working toward the Ph.D. degree at Portland State University.

He has been with Biomedical Signal Processing Laboratory since 2003. He has published four conference papers and given several public presentations. His research interest is to extract useful information from biomedical signals based on advanced signal processing techniques. He is specifically interested in analyzing various types of tremor signals obtained from patients with movement disorders and advancing the current treatments for the diseases. He is also working with a local semiconductor manufacturing company to improve a fault isolation technique based on regression algorithms.

James McNames (M'99–SM'03) received the B.S. degree in electrical engineering from California Polytechnic State University, San Luis Obispo, in 1992. He received the M.S. and Ph.D. degrees in electrical engineering from Stanford University, Stanford, CA, in 1995 and 1999, respectively.

He has been with the Electrical and Computer Engineering Department at Portland State University, Portland, OR since 1999, where he is currently an Associate Professor. He has published over 90 peer-reviewed journal and conference papers. His primary research interest is statistical signal processing with applications to biomedical engineering and semiconductor manufacturing. He founded the Biomedical Signal Processing (BSP) Laboratory (bsp.pdx.edu) in fall 2000. The mission of the BSP Laboratory is to advance the art and science of extracting clinically significant information from physiologic signals. Members of the BSP Laboratory primarily focus on clinical projects in which the extracted information can help physicians or medical devices make better critical decisions and improve patient outcome.